Available online at www.sciencedirect.com
SCIENCE DIRECT®
Tectonophysics xx (2006) xxx–xxx
TECTONOPHYSICS
www.elsevier.com/locate/tecto

Meteorological triggering of earthquake swarms at Mt. Hochstaufen, SE-Germany

T. Kraft *, J. Wassermann, E. Schmedes, H. Igel

Ludwig-Maximilians-University, Department of Earth and Environmental Sciences, Geophysics Section, Theresienstr. 41, 80333 Munich, Germany

Received 1 August 2005; received in revised form 28 October 2005; accepted 25 March 2006

Abstract

A growing body of evidence suggests that fluids are intimately linked to a variety of faulting processes. Yet, the particular mechanisms through which fluids and associated parameters influence the stress regime and thus the seismicity of a particular area are not well understood.

We carry out a study of the spatio-temporal behavior of earthquakes, fluid-related parameters (groundwater levels) and meteorological observables (precipitation) in the swarm earthquake area of Bad Reichenhall, southeastern Germany. The small volume in which the earthquakes take place, almost yearly occurring earthquake swarms and a permanent, seismo-meteorological monitoring network, provide nearly controlled experimental conditions to study the physics of earthquake swarms and to infer characteristic properties of the seismogenic crust.

In this paper we (1) describe this fairly unique study area in terms of geology, seismicity and atmospheric conditions; (2) present two cases of earthquake swarms that seem to follow above-average rainfall events; and (3) examine the observed migration of hypocenters with a simple pore pressure diffusion model.

We find significant correlation of seismicity with rainfall and groundwater level increase, and estimate an average hydraulic diffusivity of $D=0.75\pm0.35$ m^2/s for Mt. Hochstaufen in 2002.

Keywords: Seismology; Induced earthquakes; Swarms; Poroelasticity; Hydraulic diffusivity; Northern Limestone Alps

1. Introduction

By observing hydrothermal precipitants in mineral veins, mining geologist had for centuries achieved a quantitative appreciation of the role of fluid pressure in counteracting normal stress during faulting. The seminal paper by Hubbert and Rubey (1959) stands out as the foundation work in structural geology applying the concept of effective stress (Terzaghi, 1923) in a quantitative manner to faulting in fluid-saturated rock. They identified the development of fluid pressures to near-lithostatic levels as an important mechanism for lowering the strength of overthrust faults.

In recent years, hydromechanical coupling has been proposed as a possible explanation for several geological phenomena (e.g., Neuzil, 2003), including the anomalous weakness of many major faults, fault creep, slow earthquakes, or afterslip (e.g., Sleep and Blanpied, 1992; Byerlee, 1993); silent slip events

* Corresponding author. Tel.: +49 89 2180 4226; fax: +49 89 2180 4205.
E-mail addresses: Kraft@LMU.de (T. Kraft), Heiner.Igel@LMU.de (H. Igel).
URL: http://www.geophysik.uni-muenchen.de/~toni (T. Kraft).

0040-1951/$ - see front matter © 2006 Elsevier B.V. All rights reserved.
doi:10.1016/j.tecto.2006.03.044

observed by GPS surveys (e.g., Kodaira et al., 2004); seismicity patterns of aftershocks (e.g., Nur and Booker, 1972; Miller et al., 2004) and remote triggering of earthquakes by transient dynamic stress fields (e.g., Prejean et al., 2004).

Direct evidence of the effects of fluid pressure on fault stability has come from earthquakes induced in intraplate regions (e.g., reservoir induced seismicity (e.g., Howells, 1974; Ferreira et al., 1995; Talwani, 2000), fluid-injections in wells (e.g., Baisch et al., 2002; Rothert and Shapiro, 2003) and increase in hydraulic head or stream discharge connected with microseismicity (e.g., Roeloffs et al., 2003; Manga et al., 2003)).

Another phenomenon that is thought to be linked to hydromechanical coupling is the occurrence of earthquake swarms. These are sequences of earthquakes that often start and end gradually and in which no single earthquake dominates the size (Scholz, 1994). Earthquake swarms are a globally observed phenomenon and are commonly associated with volcanic regions (Sykes, 1970). The temporal evolution of swarm activity can not be described by any simple law, as e.g. the Omori law for aftershock sequences. Furthermore, the frequency-size distributions of earthquake swarms are normally characterized by unusually large *b*-values (Sykes, 1970).

Several mechanisms have been proposed for earthquake swarm generation. Mogi (1963) suggested that in highly fractured regions stress concentrations around fractures promote failure already under small stresses without the occurrence of large rupture surfaces. Other models are based on the Mohr–Coulomb failure theory in its effective stress formulation. Hill (1977) proposed a model for volcanic regions, which assumes a system of magma-filled dikes interconnected by stress-field-oriented fractures that rupture under certain pore pressure conditions in the dike. Yamashita (1999) suggested that swarm-like sequences could be created by fluid flow from localized high pressure compartments controlled by permeability increase due to fracturing.

In this study we investigate the spatio-temporal behavior of earthquakes, groundwater levels, precipitation and their correlations in the swarmquake area of Bad Reichenhall, in southeastern Germany. The aim of this

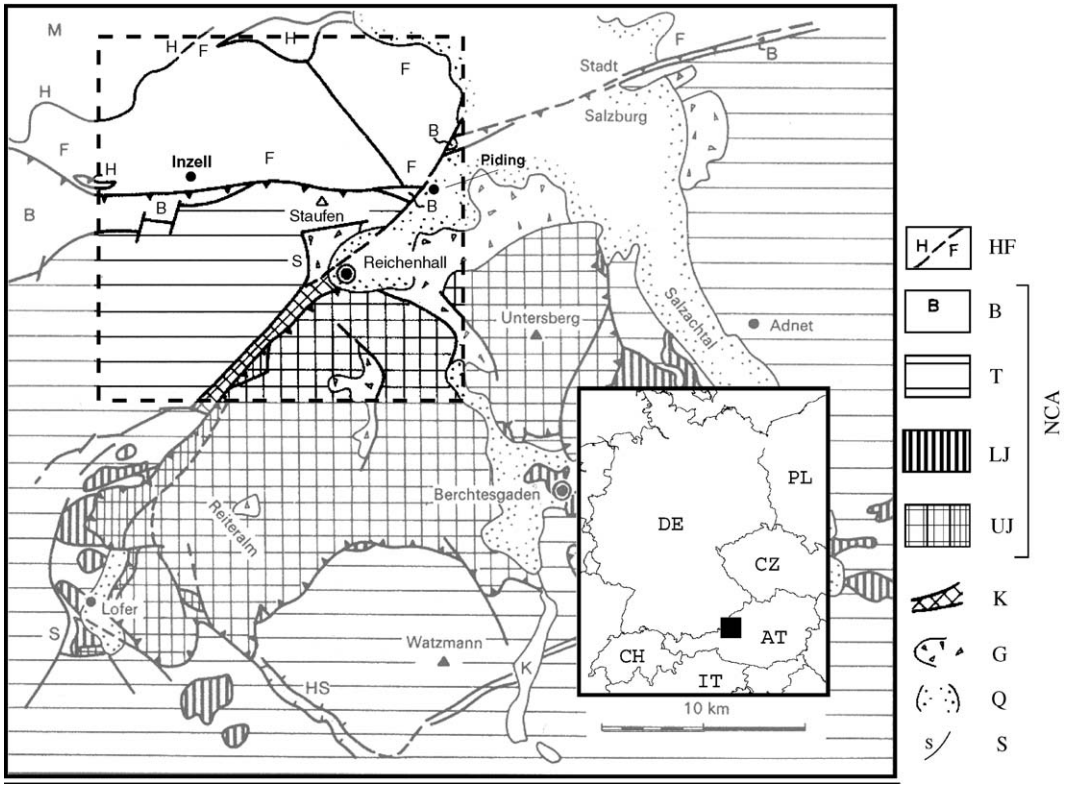

Fig. 1. Tectonic map of the region around the study area (modified from Bögel and Schmidt, 1976). The classical subdivision of the Northern Limestone Alps (**NCA**) in four nappe units is indicated. The study area is marked by a dashed square. The insert map gives the geographical location of the tectonic map. **HF** Helvetic Unit and Flysch Zone; **B** Bavaric, **T** Tirolic, **UJ** Upper and **LJ** Lower Juvavic Units; **K** Kugelbach Zone; **S** Saalach Western Fault; **G** Gossau conglomerates; **Q** Quaternary sediments.

paper is (1) to describe this fairly unique study area in terms of geology, seismicity and atmospheric conditions; (2) to present two cases of earthquake swarms that seem to follow above-average rainfall events; and (3) to examine the observed migration of hypocenters with a simple pore pressure diffusion model.

2. The study area

2.1. Geography, morphology, tectonics and geology

The Staufen Massif is an east-west striking mountain chain in southeastern Germany, northwest of Bad Reichenhall. The highest summit on this 10 km long ridge between the communities of Piding and Inzell is Mt. Hochstaufen (1775 m). Though situated directly at the morphological northern margin of the Alps, its morphology is of a remarkably High-Alpine character, which is emphasized by the high topographic gradients of the northern and southern flanks, as well as the low lying Reichenhall Basin in the south. The difference in altitude between the city of Bad Reichenhall and the summit of Mt. Hochstaufen is nearly 1200 m.

We will only briefly outline the tectonic setting and the geology of the Staufen Massif, a detailed description can be found in e.g., Erhardt (1931), Henrich and Zankl (1981) and Weede (2002). The Northern Limestone Alps (NCA), a part of the Austroalpine Mega-Unit, are an elongate fold-and-trust belt with a complex internal structure and are classically subdivided into four nappe units: the Bavaric, Tirolic, Lower- and Upper Juvavic Units (Fig. 1, for details e.g., Tollmann, 1976). The Staufen Massif is part of the Tirolic facies, which overthrusted the intensely folded Bavaric Unit. In the eastern part of the Staufen Massif the Bavaric Unit was completely traversed. There, the Tirolic Unit is in direct contact with the Flysch Zone in the North. The southern border to the Juvavic Units is build by the northeast striking Saalach Western Fault and Kugelbach Zone. The later widens in the east to form the Reichenhall Basin with salinar sequences of remarkable thickness, which explain the increased mobility of the tectonic units in the region (Zankl and Schell, 1979).

The Staufen Massif is made up of a stratigraphic sequence from the lower to middle Triassic (Fig. 2). It predominantly consists of limestone and dolomite, which in some stratigraphic units alternate with marl, clay and sandstone. The summit region consists of Wettersteinkalk (limestone), which shows distinct signs of Karst formation. Haselgebirge, a leached and weathered breccia of evaporitic permo-triassic sediments, can be found in some outcrops on the northern flank of the Staufen Massif and in the Reichenhall Basin. Presumably, Haselgebirge also exists in the innermost fold cores of the Staufen Massif (Weede, 2002). A schematic cross section and stratigraphy of Mt. Hochstaufen is shown in Fig. 2.

Geologic evidence for mass movements at the southern flank of Mt. Hochstaufen was recently summarized by Weede (2002). Large east-west striking open fractures can be found near the summit of Mt. Hochstaufen. They reach a length of several hundred

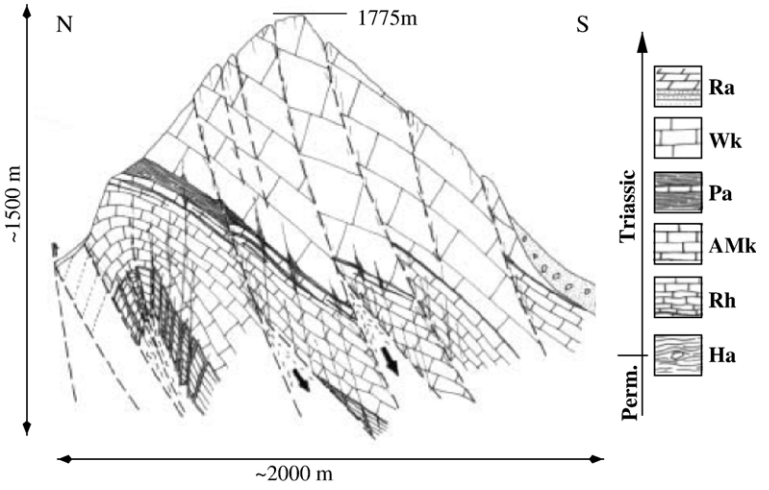

Fig. 2. Schematic geological cross section of Mt. Hochstaufen (modified from Weede, 2002). Ra: Raibler Formation; Wk: Wettersteinkalk (Limestone); Pa: Partnach Formation; AMk: Alpine Muschelkalk (Limestone); Rh: Reichenhall Formation. For a detailed lithology refer to Henrich and Zankl (1981).

meters and openings of up to 3 m. Speleologists were able to follow those fractures to a depth of nearly 100 m below the surface (Glaser, 2004). Gravitational collapse and/or subsidence due to leaching of the Haselgebirge are debated as causative processes.

2.2. Previous studies and seismicity

Reports of felt earthquakes in the area of Bad Reichenhall range back to October 16th, 1390, which is also the first record in the Bavarian earthquake catalog. Although the list of macroseismically observed earthquakes is certainly not complete, all of the 30 reported events (Fig. 3) were surely only felt in the vicinity of the city of Bad Reichenhall. The maximum intensity reached was $I_0 = V$ on the macroseismic scale. As illustrated in Fig. 3, the majority of these earthquakes occurred in the summer months which are also characterized by having the highest average precipitation values. This observation and the confined anomalous character of the seismic activity encouraged first interpretations considering the local geological setting. Giessberger (1918) proposed cavity collapses caused by solution of salt from the Haselgebirge formation in the Reichenhall Basin as a causative mechanism. Schmedes (1979) additionally suggested corresponding processes during Karst formations of the Lattengebirge mountains in the south and gravitational subsidence of the overlying rock due to leaching of the Haselgebirge formation.

In February 1972 a short period seismometer was installed in the old salt refinery in Bad Reichenhall. The instrument had only a vertical component which did not allow earthquake location or determination of focal mechanisms. Nevertheless, Schmedes (1979) was able to verify the temporal pattern in seismic activity characterized by relative quiescence in the beginning of the year and an annual maximum in summer. He also reported for the first time on the occurrence of earthquake swarms in the Bad Reichenhall area.

A mobile network consisting of digital seismograph stations was installed in a widespread area around Bad Reichenhall in 1978 (Schmedes, 1979). Using data of this network from the time period from 1978 to 1980, Nöthen (1981) showed that the seismicity of the study area was mainly concentrated in the Staufen Massif north of Bad Reichenhall. He concluded from calculated

a)

origin time	I_0
1390/10/16 :	5.0
1906/06/13 07:54	3.5
1910/11/19 11:20	4.5
1919/08/18 03:33	4.0
1920/02/05 17:18	4.0
1920/09/27 11:03	5.0
1924/06/19 19:45	4.0
1928/10/06 06:40	4.0
1933/02/06 22:50	4.0
1938/06/12 14:45	5.0
1942/02/18 14:00	4.0
1943/03/20 03:30	4.0
1965/07/09 22:48	5.0
1977/10/02 15:29	
1977/12/28 09:21	3.0
1978/05/07 15:32	4.5
1979/08/04 22:24	5.0
1980/05/07 19:38	3.0
1980/05/17 16:31	5.0
1980/07/11 06:43	
1980/07/29 19:15	5.0
1995/05/22 19:00	3.0
1995/06/26 17:43	4.0
1995/06/27 17:16	4.0
1995/09/10 07:49	4.0
1999/05/15 05:34	4.0
1999/05/22 21:35	
1999/05/26 20:16	3.0
2000/05/20 13:11	3.0
2005/07/18 14:46	3.0?

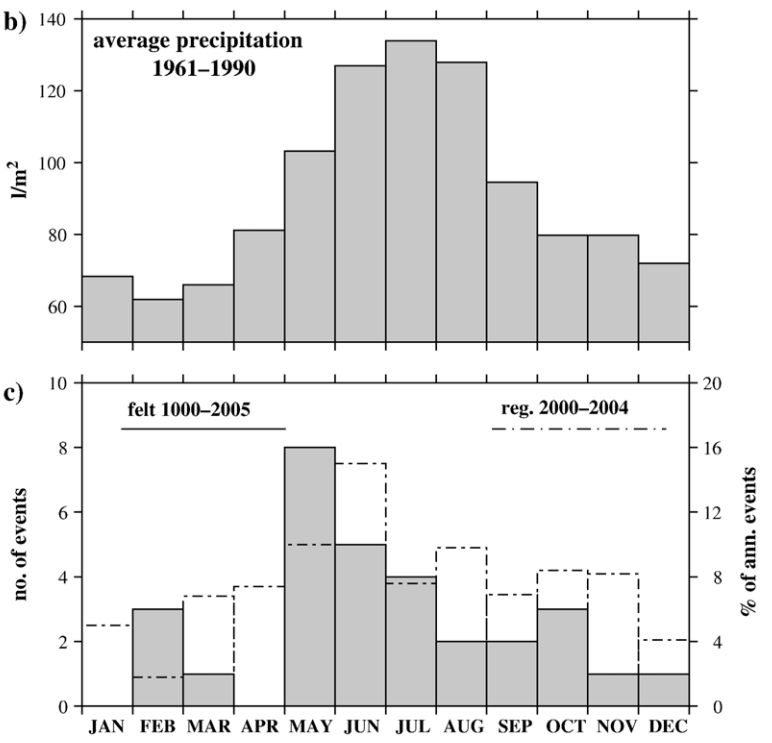

Fig. 3. Macroseismicity of the Bad Reichenhall area between 1000 and 2005. a) List of origin time and maximum macroseismic intensity I_0 of earthquakes reported felt in Bad Reichenhall. b) Precipitation in the reference period 1961 to 1990 for the Alps (Fuchs et al., 1999). c) Histogram of earthquakes in a) and dash dotted histogram of monthly percentage of annually registered earthquakes between 2001 and 2004 at station STAU.

focal mechanisms that tectonic slip events dominate the seismicity and excluded the earlier proposed explanation of cavity collapses.

On June 26th, 1995, a magnitude ML=2.7 earthquake was located and felt in Bad Reichenhall. The next day the University of Munich installed a dense mobile seismological network around the Staufen Massif. In a detailed study of the recorded data of the 2 months deployment time Schwarzmann (1996) found that the seismicity is confined to shallow depth (above 2.5 km) and concluded from the variety of calculated focal mechanisms that it was bound to different independent fault planes. She also found weakly significant (c_{max}=0.6, c_{max}: maximum cross-correlation coefficient) and close correlation (c_{max}=0.8) of seismicity with precipitation and associated groundwater level for a 15 years period starting in 1980, and suggested a causal connection between seismicity and rainfall in the study area.

However, what was missing is a long-term observation of the Bad Reichenhall area in terms of seismicity, meteorological parameters and associated hydrological observables. Only the recording of complete swarm sequences by such a dense and permanent "seismo-meteorological" network can help to identify and understand the processes that drive swarm-type seismicity in the Staufen Massif.

2.3. Seismo-meteorological network

Previous studies, mentioned above, have emphasized the need of multi disciplinary and permanent monitoring of the Bad Reichenhall area. Beginning in 2001 a "seismo-meteorological" network was installed in the study area. It consists of three parts which are described in the following.

2.3.1. Seismology

In 2001, the University of Munich in cooperation with the Geological Survey of the Bavarian State installed a new seismological network in Bavaria. It now consists of 21 stations which send their data in near real time to the data center in the Geophysical Observatory in Fürstenfeldbruck via telephone line. A subnet consisting of six short period stations was installed around the Staufen Massif.

To close some gaps in the station coverage, arising from the high level of infrastructure required for the permanent stations (power and telephone lines), we installed three additional mobile stations starting in mid-April 2002. All mobile stations were deployed in open field close to the source region of the swarm-earthquake activity. Data was recorded in continuous mode with a sample rate of 125 Hz and 200 Hz. All station locations are given in Fig. 4.

2.3.2. Meteorology

The German Weather Service (DWD) operates a dense network of meteorological stations in Germany. In our study area four pluviometer stations are available. Precipitation is read off manually every 24 h at 6:30 local time. Data of these stations was made available by the DWD in digital form. A map of all stations can be found in Fig. 4.

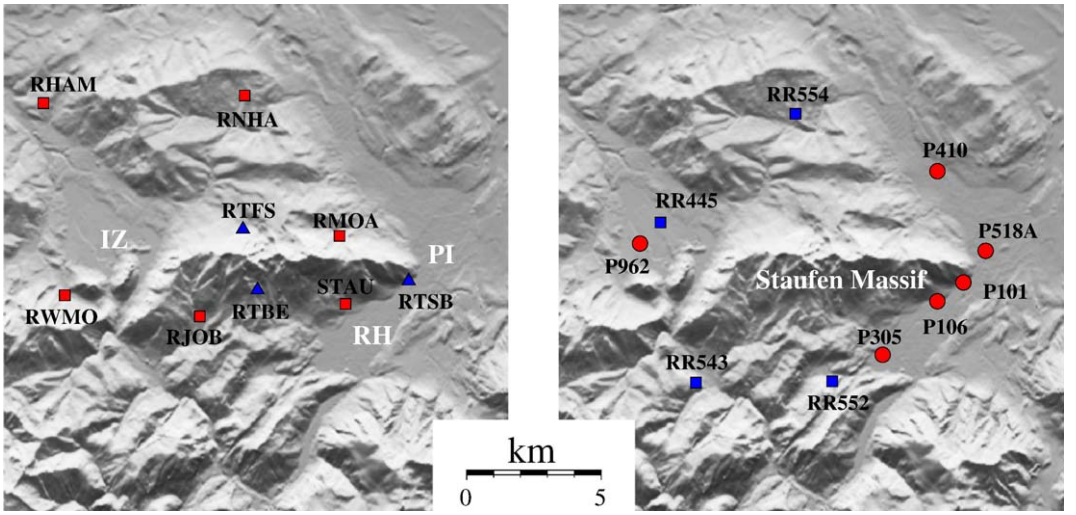

Fig. 4. Seismo-meteorological network around Mt. Hochstaufen. Map borders: lon. 12°40′–12°57′ E; lat. 47°40.5′–47°55.5′ N. Left: Map of permanent (squares) and mobile (triangles) seismological stations recording in 2002. The cities Inzell (IZ), Piding (PI) and Bad Reichenhall (RH) are indicated. Right: Hydrological (circles) and meteorological (squares) stations.

2.3.3. Hydrology

The Bavarian Bureau of Water Resources (WWA) and the SüdSalz GmbH (SUD, salt refinery in Bad Reichenhall) provided data of groundwater gauges located around the Staufen Massif. The wells are between 5 and 50 m deep. The three shallow wells operated by the WWA in our study area register the groundwater level on paper records. In the Bad Reichenhall basin the groundwater level in several deep wells is read off by SUD manually on a daily basis.

The data was provided in the form of error-corrected plots, which were scanned and digitized for further analysis. The resolution of both datasets is 1 cm in groundwater level and approximately 1 day in time. All groundwater well positions are given in Fig. 4.

Information on station coordinates and instrumentation as well as access to near-real time seismograms is available via Internet (www.erdbebendienst.de).

3. The 2002 earthquake swarms

In March and August 2002, intense rainfall events led to severe flooding in Central Europe, causing an economic damage of 18.5 billion Euro (Munich Re Group, 2003). Precipitation in the study area exceeded the monthly average within 48 h, respectively 24 h, during these events. The seismicity in the Hochstaufen mountain range increased significantly after both rain events. A detailed analysis of the resulting earthquake swarms, which were recorded with the "seismo-meteorological" network, will be presented in the following.

3.1. Data analysis, derivation of velocity model

An event list generated automatically at station STAU (southern flank, permanent) and manually at station RTFS (northern flank, mobile) built the basis for the extraction of local earthquakes (epicentral distances smaller than ~15 km) from the continuous recordings. Extracted waveforms were usually 1 min in length, and stored in an event database in GSE format using the software package GIANT (Rietbrock and Scherbaum, 1998).

We manually picked arrival-times of P- and S-phases for all recorded earthquakes. The accuracy of the best readings reached the sampling distance (0.05–0.08 s). Weights from 0 (best) to 4 (neglected; uncertainty >0.3 s) were assigned to the arrival-times. Local magnitudes were calculated after Bakun and Joiner (1984). Estimates of hypocentral distance from the difference of arrival-times of the P- and S-phases allowed magnitude estimates for events recorded only at one station. Such events were identified as being local earthquakes by the similarity to waveforms of events recorded on more than one station.

A homogeneous half space velocity model was derived in a coupled hypocenter velocity inversion using the VELEST algorithm (Kissling et al., 1994) for well determined events. These were defined by having a

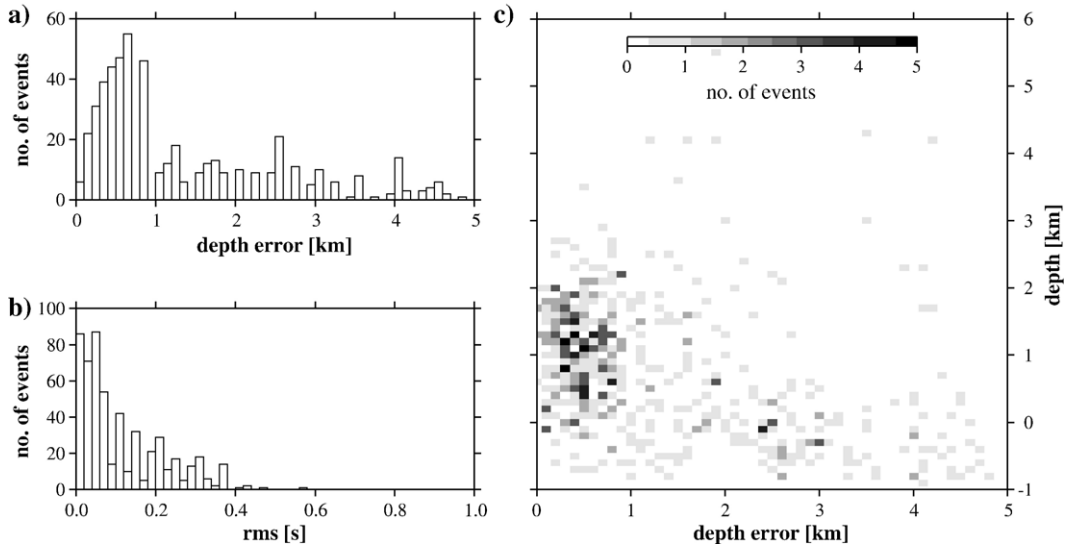

Fig. 5. Location error obtained with Hypo71 (Lee and Lahr, 1975) and the *minimum-1D-velocity model* for Mt. Hochstaufen earthquakes in 2002. Histogram of a) root-mean-square (rms) error sum of differences between and calculated observed travel times, and b) depth error. c) Scatter plot of depth error versus hypocenter depth.

station gap <180° and a number of travel time observations ≤6, and were found in repeated VELEST runs. The resulting so-called *minimum-1D-velocity model* (v_p=5.6 km/s; v_s=3.1 km/s; v_p/v_s=1.81) represents the least-squares average velocity of the region that is sampled by seismic rays (Kissling et al., 1994). The derived velocity model oversimplifies the velocity structure of the study area. However, we think its use is justified for a standard earthquake location because the seismicity and the seismological network are predominantly confined to one lithological unit (Northern Limestone Alps), having a small source volume, and a close station spacing respectively.

The *minimum-1D-velocity model* was used for standard earthquake location with the program Hypo71 (Lee and Lahr, 1975). 546 earthquakes with a minimum of six observed arrival-time readings could be located. As topography was not taken into account, the calculated depth $d_{H71}(j)$ represents the depth below the average elevation $\Delta_{mean}(j)$ of the stations contributing to the solution. The absolute depth $d(j)$, which is used in the following, is then calculated for each event j as $d(j)=d_{H71}(j)-\Delta_{mean}(j)$. The overall mean station elevation is −793 m (depth positive down).

Fig. 5 illustrates the location quality obtained for the 2002 Hochstaufen earthquakes. The root-mean-square (rms) errors of the differences between calculated and observed travel times are small, mainly below 0.1 s (Fig. 5b), and indicate good quality of onset-time determination. For the majority of the events the depth errors, calculated with Hypo71 (Lee and Lahr, 1975), is less than 1 km (Fig. 5a) indicating fairly good location results. Greater errors are observed especially for very shallow events above and slightly below sea level (Fig. 5c). This is due to the fact, that for shallow events the relative travel time error is larger than for deep events, because the travel times become very short. In the following derivation of hydraulic parameters we will therefore introduce weighting and neglect events with depth errors greater than 3 km.

3.2. Observed seismicity

In 2002, 1171 earthquakes were recorded in the study area. The strongest event had a magnitude of ML=2.4 on April 10. From the magnitude–frequency statistics we assume the recorded dataset to be complete down to a magnitude of ML=−0.5. The epicenters of the located events are diffusely distributed over the Staufen Massif (Fig. 6). Their source depths rarely exceed 3 km below sea level (Fig. 7d). We estimated the stability of the location result by relocating the events using different

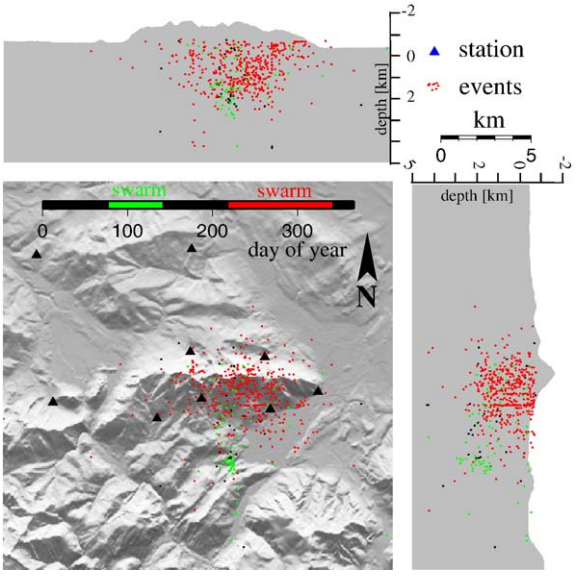

Fig. 6. Epicenters of 546 earthquakes in 2002 located using Hypo71 (Lee and Lahr, 1975) and the derived *minimum-1D-velocity model*. Colors identify two swarm-earthquake periods. Green: March swarm (~80 events); red: August swarm (~430 events); black: background seismicity (~40 events). Triangles mark seismological stations installed in 2002. Map borders: lon. 12° 40′–12° 57′ E; lat. 47° 40.5′–47° 55.5′ N. E–W and N–S profiles through the summit of Mt. Hochstaufen (1775 m).

initial hypocenters. For the majority of the events a lateral change of less than 500 m was observed.

The spatio-temporal behavior of the seismicity is illustrated in Fig. 7. Fig. 7a displays the mean of four pluviometers operated by the DWD in the study area (see Fig. 4). Most of the events can be assigned to swarmquake phases in March and August, which were following above-average rainfall events. Both events were characterized by exceeding the monthly average of precipitation within 48 h, and 24 h respectively. The number of earthquakes per day in Fig. 7b illustrates the seismic activity. It increased roughly coincident with the onset of the intense rain events. In both cases seismicity reached its maximum approximately 10 days after their onsets and stayed on an elevated level for several weeks.

The first swarm in March was mainly concentrated on a small volume of approximately 1 km^3. The centroid was located further south and in a significantly less elevated region as usually observed in earlier studies and for the subsequent swarms in August (see Fig. 6). This may be due to the fact that precipitation in the elevated parts of the study area fell as snow or an interaction of the beginning snowmelt with the intense rainfall in the lower part of the study area.

The second earthquake swarm starting in August can be divided into three sub-swarms. The first one contains

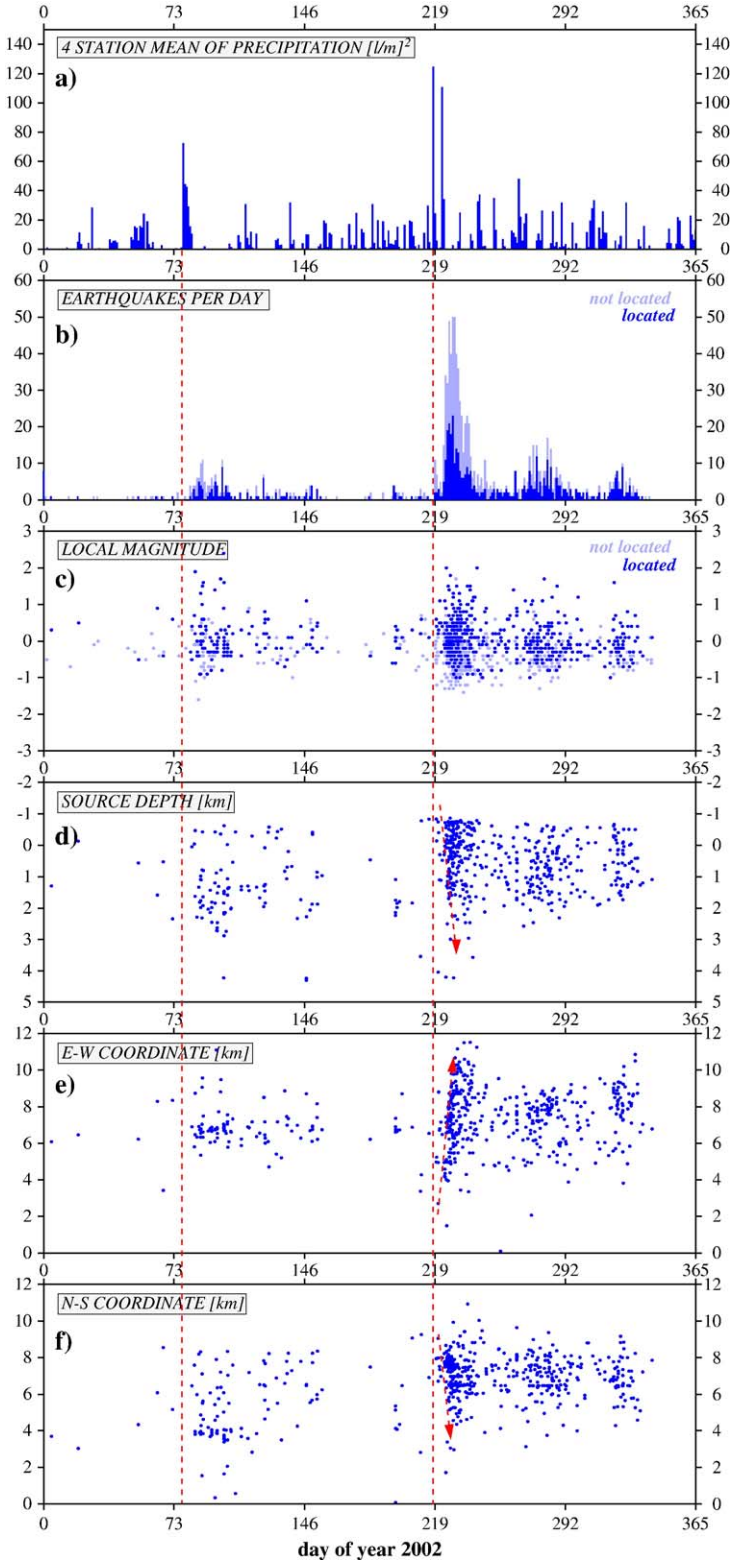

Fig. 7. Spatio-temporal development of the seismicity in 2002. Vertical red lines mark the onsets of intense rain events in March and August. Red arrows illustrate the migration of hypocenters with time into depth (d), to the east (e), and to the south (f) for the first sub-swarm in August. (For interpretation of the references to colour in this figure legend, the reader is referred to the web version of this article.)

most of the recorded earthquakes. Within this sub-swarm the data suggests a migration of hypocenters over time. From very shallow depth west of the summit region of Mt. Hochstaufen they move to depths of 2.5 km in a southeast direction within about 5 days. The hypocenter migration is illustrated by red arrows in Fig. 7d–f. The increased seismicity makes it difficult to clearly identify a similar behavior for the following sub-swarms.

However, as illustrated in Fig. 8 each swarm and sub-swarm can be associated with an event of strong rainfall, as well as increasing groundwater level. To assure the comparison of evenly sampled time series within comparable frequency bands, we preprocessed the time series of precipitation (R, Fig. 7a), seismicity (EG, Fig. 7b), and groundwater level increase rate (ΔG^+) with Gaussian filters of different lengths (see Table 1). Further, lower threshold levels (see caption to Fig. 8) were introduced to reduce uncorrelated background noise. Fig. 8 visualizes the resultant normalized time series for a filter length of 10 days as color coded horizontal bars. The seismicity bar was time shifted by 10 days according to best-lagged cross-correlation result (see Table 1). Clearly the good temporal agreement of maxima in the different time series (vertical white stripes) can be seen.

The quantitative results of the cross-correlations for the different time series preprocessed with different filter lengths are given in Table 1. Best time lags between 9 and 11 days for seismicity against precipitation and ΔG^+ are obtained. Precipitation and ΔG^+ correlated best with zero delay. The cross-correlation coefficients (c_{max}) increase with increasing filter length due to smoothing of the time series. Consequently however, the accuracy of the delay time estimation decreases. To balance this tradeoff for visualization we choose a filter length of 10 days in Fig. 8, which results in $c_{max}>0.70$ for all time series and still allows their detailed comparison.

Cross-correlation analysis assumes a linear relation between time series, which can only be a first order approximation in our case. However, the significant correlation of seismicity with precipitation and ΔG^+, and its time delay of 9–11 days suggest, that diffusive hydraulic processes can trigger swarm-type earthquake activity in the Staufen Massif. We will discuss a possible mechanism in the following.

Table 1
Cross-correlation result for precipitation R, seismicity EQ, and increase rate of groundwater level of well P518A in Piding (see Fig. 4) ΔG^+ for 2002

Gauβ	1	4	8	10	15	20
EQ/R	9	9	10	10	11	11
	(0.44)	(0.55)	(0.74)	(0.78)	(0.83)	(0.87)
EQ/ΔG^+	9	9	10	10	11	11
	(0.47)	(0.60)	(0.67)	(0.72)	(0.78)	(0.83)
R/ΔG^+	0	0	0	0	0	0
	(0.66)	(0.89)	(0.94)	(0.94)	(0.95)	(0.95)

Time series are Gaussian filtered (length of filter in days is given in the first row). Lower thresholds: R: 8%; EQ: 2%; ΔG^+: 18% were applied. Best time lags in days and corresponding maximum cross-correlation coefficient (in parenthesis) are given.

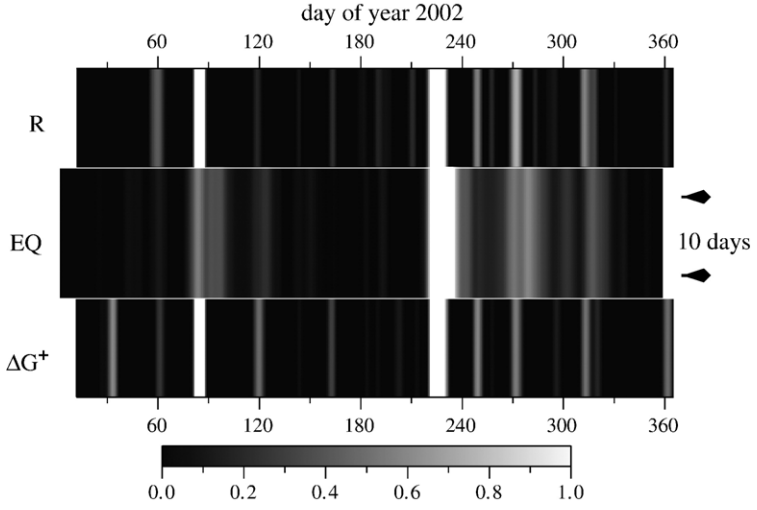

Fig. 8. Gray scaled normalized time series of precipitation R, seismicity EQ, and increase rate of groundwater level of well P518A in Piding (see Fig. 4) ΔG^+ for 2002. Time series are Gaussian filtered (10 days). Lower thresholds: R: 8%; EQ: 2%; ΔG^+: 18% (and upper threshold for this figure: EQ: 50%) were applied. EQ is time shifted by 10 days for maximum correlation (compare Tab. 1). The gray scale used is indicated.

4. Hydrological interpretation

It is widely accepted, that increase in pore fluid pressure reduces the shear strength of a porous medium by counteracting normal stress. This is known as the concept of effective stress originally formulated by Terzaghi (1923). If a porous medium is stressed to nearly critical values even a small increase of pore pressure can provoke failure (e.g., Segall, 1985; Roeloffs, 1988; King et al., 1994; Harris, 1998).

Pore pressure diffusion as a triggering mechanism has been proposed for many case studies; e.g., aftershocks of strong earthquakes (e.g., Nur and Booker, 1972; Bosl and Nur, 2002; Shapiro et al., 2003), reservoir induced (e.g., Howells, 1974; Ferreira et al., 1995; Talwani, 2000), and fluid-injection induced (e.g., Shapiro et al., 1997; Rothert and Shapiro, 2003) earthquakes, changes of water table or stream discharge connected with microseismicity (e.g., Costain and Bollinger, 1991; Lee and Wolf, 1998; Braitenberg, 2000), intraplate earthquake swarms (e.g., Parotidis et al., 2003), as well as observations of seasonality in seismicity correlated with snowmelt (e.g., Wolf et al., 1997; Saar and Manga, 2003) or precipitation (e.g., Roth et al., 1992; Muco, 1995, 1999; Ventura and Vilardo, 1999).

We also assume that pore pressure diffusion is a possible mechanism for triggering swarm activity in our study area. Consequently, as a first step we model the intense rain events as step increases in fluid pressure at the surface of a homogeneous half space and consider one-dimensional diffusion only. In doing so we will follow the notation and definition given in the review paper by Kümpel (1991).

The time-dependent interaction of fluid flow and rock deformation is described by the theory of poroelasticity (Biot, 1962). In a source free, homogeneous half space, with scalar hydraulic diffusivity D, the low frequency evolution of pore pressure P due to irrotational flow can be described by the diffusion equation (e.g., Wang, 2000):

$$\frac{\partial P}{\partial t} = D\nabla^2 P. \tag{1}$$

For a periodic pore pressure variation $P(0, t)=P_s\exp(i\omega t)$ at the surface of the half space the solution to Eq. (1) is given by (e.g.,Wang, 2000, pp.140–143):

$$P(z,t) = P_s \exp\left(-z\sqrt{\frac{\omega}{2D}}\right)\exp\left(i\omega\left(t-\frac{z}{\sqrt{2\omega D}}\right)\right) \tag{2}$$

This is a plane wave with attenuation coefficient equal to $\sqrt{\omega/2D}$ and with a velocity of $\sqrt{2\omega D}$, where z is depth, t is time and ω angular frequency. An estimate of diffusivity D can be obtained using the following logic, originally formulated by Shapiro et al. (1997): A first order approximation of the injection signal (increase of pore pressure at the surface due to intense rainfall) is a rectangular pulse starting at the same time as the rain event $t=0$ and ending at some time $t=t_e$ after the end of precipitation. However, for an earthquake triggered at time $t=t_0$ the evolution of the injection signal for times $t>t_0$ is not relevant. Hence, for this event the injection signal duration can be set to t_0. The dominant frequencies of the power spectrum of a rectangular pulse with duration t_0 are in the range $0 \le \omega \le 2\pi/t_0 \equiv \omega_0$. From Eq. (2) one finds that the propagation velocity of pore pressure variations is proportional to $\sqrt{\omega}$. Further, we expect that even a small increase in pore fluid pressure can trigger seismicity. Consequently, we set $\omega=\omega_0\equiv 2\pi/t_0$ to calculate the velocity of a triggering front behind which seismicity can be induced from Eq. (2). Doing this for the time range $t_0 \in [0, t]$ we find the time-depth dependence of the triggering pore pressure front:

$$z = \sqrt{4\pi D t}. \tag{3}$$

Hydraulic diffusivity can now be estimated by finding the triggering front parabola from Eq. (3) that best separates the area of elevated seismicity from the background seismicity in a time-depth plot.

Fig. 9 shows time-depth plots for the intense rain events of March 19th, August 6th, September 23rd, and a stack of the three, including all located earthquakes of the following 40 days. This time window length was chosen to separate the sub-swarms in August. Delays between the rain events and the increase of seismicity seem to be indicated in Fig. 9a–d. However, a comparison with Fig. 7b shows, that these gaps arise from the lack of locatable events for that time. The delayed seismicity of the March swarm can be observed in both figures. There are several possible explanations for this which will be discussed below. The fraction $f_{eq}(D)$ of events below the triggering front parabola was calculated as a function of diffusivity D in the range $0.05\ \mathrm{m^2/s} \le D \le 5\ \mathrm{m^2/s}$. Weights ($w=\frac{3-\Delta z}{3}$) were applied according to the depth location error Δz, and events with $\Delta z \ge 3$ km were neglected. In a semi logarithmic plot $f_{eq}(D)$ can be approximated by two straight lines (Fig. 9e), whose intersection point corresponds to the best estimate of D. The method was verified using different synthetic data sets composed of randomly distributed data points obeying the depth dependence in Eq. (3) and random background noise of different levels. The best fitting

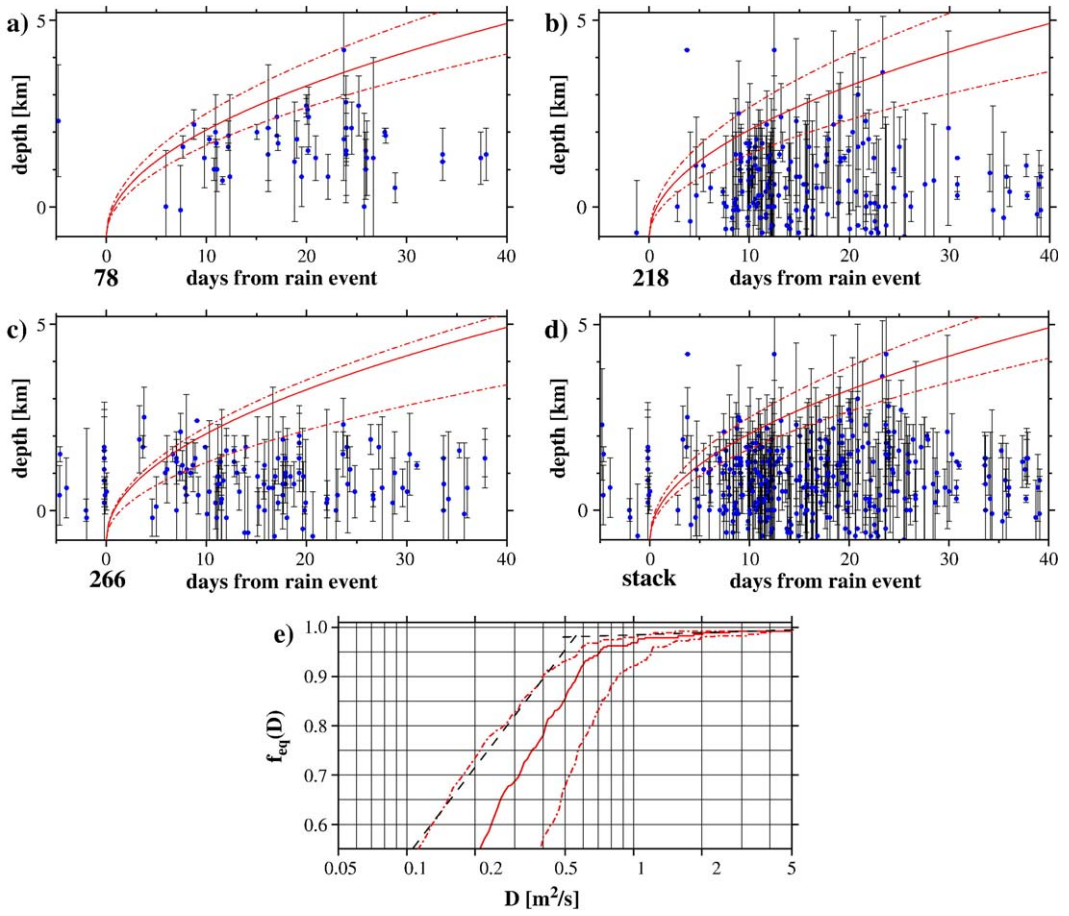

Fig. 9. Time-depth plots for three earthquake swarm of 2002. Depth uncertainties due to standard earthquake location are indicated by error bars. Best fitting parabolas are shown for located depth plus error, located depth, and located depth minus error. a) March 19th (day of year (day) 78). D: 1.0 m^2/s, 0.75 m^2/s, and 0.55 m^2/s. b) August 6th (day 218). D: 1.1 m^2/s, 0.75 m^2/s, and 0.45 m^2/s. c) September 23rd (day 266). D: 0.85 m^2/s, 0.75 m^2/s, and 0.4 m^2/s. d) Stack of a, b, and c. D: 1.0 m^2/s, 0.75 m^2/s, and 0.55 m^2/s. e) Fraction $f_{eq}(D)$ of events below the triggering front parabola for stacked rain events ($D \in [0.05\ m^2/s, 5\ m^2/s]$). Dashed lines approximate $f_{eq}(D)$ (here e.g., upper error estimate), intersection point gives best estimate for D.

parabolas are superimposed on the time-depth diagrams in Fig. 9a–d. We find a value of $D \simeq 0.75\ m^2/s$ in all investigated cases. Upper and lower error estimates for hydraulic diffusivity were derived by repeating the described algorithm for data sets with Δz added and subtracted. Extreme values for D are obtained for August 6th ($D = 1.1\ m^2/s$) and for September 23rd ($D = 0.4\ m^2/s$).

5. Discussion and conclusion

The observations and first interpretations presented above indicate that seismicity in the Staufen Massif is influenced and partially even triggered by meteorological parameters. This is true for the long-term behavior of seismicity, as well as for episodical swarm-type activity as e.g., in March and August of 2002.

The comparison of long-term precipitation and seismicity in Fig. 3 reveals the similarity in the annual record of both observables. The highest seismic activity is observed in the summer months, which are characterized by having the highest annual precipitation (Fig. 3b, c). The macroseismic record has insufficient events to be statistically significant. However, a maximum seems to develop in May, which precedes the maximum precipitation. An explanation might be, that larger earthquakes are more likely to occur after periods of relative quiescence (the winter months) during which stress decomposition by small shocks is reduced. In Fig. 3 also the maximum of the recorded seismicity seems to be ahead of the long-time average of the precipitation with a maximum in June. However, this may only reflect the fact that the time range for the recorded seismicity is much shorter than that for precipitation. Whether a

similar explanation as given for macro-seismicity above holds for microseismicity can not be answered until continuously recorded seismicity is available for a comparable range of time.

The high correlation of short-term episodical intense rainfall events and swarmquake activity in 2002 is illustrated in Fig. 8. Almost every rain event matches a corresponding event in the time-shifted seismicity record. Nonlinear coupling of seismicity and precipitation as well as groundwater level increase is most likely, because of the observed variances of delay times and amplitudes of the individual events. Furthermore, there are precipitation events and groundwater level increases that are not followed by seismicity. Possibly some are to weak to trigger earthquakes (e.g., day of year (day) 210), others might be too close to preceding events that already reduced the available stresses and the medium needs more time to develop into a critical state again (e.g., day 250).

We have shown that precipitation and groundwater level increase show maximum cross-correlations with seismicity when delayed by 9–11 days. However, the time series are dominated by the two major peaks in March and August. The result is therefore only significant for these events. More sophisticated techniques have to be applied in future analysis to decipher the nonlinear coupling relations.

The increase of seismicity in March seems to be delayed by 6 days relative to the rain event on March 19th. This might have several reasons. (1) The mobile stations were for the first time installed in mid-April 2002, therefore the sensitivity of the network may have been reduced before that time. (2) In March, snow covered the elevated parts of the mountain, and the delay may also reflect differences in the catchment region compared to the August swarms. (3) The main source region for the March swarm is offset to the south and deeper than the average seismicity in the August swarm. This region might in the upper part not be as sensitive to pore pressure changes as Mt. Hochstaufen. The data set of 2002 does not allow to distinguish between the different possibilities, and future studies have to answer this question.

The maximum depth of the main seismic activity seems to be correlated with the base of the Northern Limestone Alps. Present knowledge suggests that this overthrust fault lies at a depth of ~3 km (Angenheister et al., 1972; Will, 1975), which corresponds well with the observed seismicity. Whether diffusion is hindered by an impermeable interface at this depth or if the medium is further from a critical state in the region beneath this boundary can so far only be a speculation.

The maxima of the earthquake swarms on the other hand seem not to be correlated with any structural feature. The Fig. 7d–f, showing the spatio-temporal evolution of seismicity, should give an indication if such a correlation would exist. At the present stage, location uncertainties may be disguised as small-scale structural features, but, as discussed below, our data set offers the opportunity to apply relative-relocation techniques which will hopefully sharpen our view in the future.

We have presented a hydrological interpretation of the observed hypocenters depth-migration and derived hydraulic diffusivity $D = 0.75 \pm 0.35$ m^2/s. Additional uncertainty may arise from the fact, that we did not try to separate fluid induced and background seismicity at this stage, which can be achieved on a statistical basis (Hainzl and Ogata, 2005). However, our estimate corresponds well with results obtained by other researchers from analysis of seismicity patterns by pore pressure diffusion modeling (e.g., Ventura and Vilardo, 1999; Parotidis et al., 2003; Saar and Manga, 2003; Rothert and Shapiro, 2003; Hainzl and Ogata, 2005; Parotidis et al., 2005). These results range between 0.1 m^2/s and 10.0 m^2/s.

As already mentioned, our simplified hydrological model can only represent a first order approximation and the derived D has to be understood as an average over the studied volume. In the complex geological setting of the Staufen Massif D has to be calculated in the form of an anisotropic tensor (e.g., Rothert and Shapiro, 2003), and probably has a highly heterogeneous character. Furthermore, D might not be constant in time, because dynamic rupture can change porosity and increase permeability (e.g., Miller et al., 2004).

In order to improve the hydrologic model in these directions a more precise earthquake location is essential. Our dataset includes many events characterized by very similar waveforms, which can be used to calculate highly accurate relative earthquake locations (e.g., Fremount and Malone, 1987; Poupinet et al., 1984) and to improve the velocity model (e.g., Zhang and Thurber, 2003). Integrating data of a very dense seismometer network operating in Summer 2004, these techniques will allow to sharpen the pattern of seismicity.

As a final remark we want to report, that on July 15th, 2005, an intense rain event comparable to the August 2002 event triggered an earthquake swarm in the Staufen Massif. It was accompanied by a magnitude ML = 2.7 earthquake on July 18th, which was felt in Bad Reichenhall. Until the end of July more than 200 microearthquakes were recorded.

Acknowledgements

This study was to a major part supported by the Bavarian Ministry for Environment and by the Geological Survey of the Bavarian State. Toni Kraft was partially supported by the German Research Foundation (DFG) and the EU Community initiative INTERREG III B Alpine Space Programme SISMOVALP. Data were provided by the German Weather Service, SüdSalz GmbH in Bad Reichenhall and the Bavarian Bureau of Water Resources in Traunstein. We thank the Bavarian Forest Administration for permitting the installation of mobile stations and access to forest roads. Special thanks are expressed to the communities of Bad Reichenhall, Inzell, Piding, Teisendorf, and Siegsdorf, to the tourist club "Die Naturfreunde", as well as to Mr. Waigl and Mrs. Kerkmann for their permission to install seismological stations on their properties. Special thanks for the support, accommodation and the good times goes to "Hansi" Pauli and to the landlord and landlady of the Stoaneralm. We like to thank the following persons for giving logistic and technical support throughout the study and field campaign: Werner Bauer, Peter Danecek, Teresa Reinwald, Dr. Martin Beblo, Martin Feller, Dr. Erwin Geiβ, Gunnar Jahnke and Christian Verard.

We thank Tomas Fischer, an anonymous reviewer and Sebastian Hainzl for their helpful comments, which improved the original version of the manuscript.

References

Angenheister, G., Bögel, H., Gebrande, H., Giese, P., Schmidt-Thome, P., Zeil, W., 1972. Recent investigations of surficial and deeper crustal structures of the Eastern and Southern Alps. Geol. Rundsch. 61 (2), 349–395.

Baisch, S., Bohnhoff, M., Ceranna, L., Tu, Y., Harjes, H.-P., 2002. Probing the crust to 9-km depth: fluid-injection experiments and induced seismicity at the KTB super-deep drilling hole, Germany. Bull. Seismol. Soc. Am. 92 (6), 2369–2380.

Bakun, W., Joiner, W., 1984. The ML scale in central California. Bull. Seismol. Soc. Am. 74, 1827.

Biot, M., 1962. Mechanics of deformation and acoustic propagation in porous media. J. Appl. Phys. 33 (4), 1482–1498.

Bögel, H., Schmidt, K., 1976. Kleine Geologie der Ostalpen. Ott Verlag Thun, Switzerland.

Bosl, W., Nur, A., 2002. Aftershocks and pore fluid diffusion following the 1992 Landers earthquake. J. Geophys. Res. 107 (B12), 1–12.

Braitenberg, C., 2000. Non-random spectral components in the seismicity of NE Italy. Earth Planet. Sci. Lett. 179, 379–390.

Byerlee, J., 1993. Model for episodic flow of high-pressure water in fault zones before earthquakes. Geology 21, 303–306.

Costain, J.K., Bollinger, G.A., 1991. Correlation between streamflow and intraplate seismicity in central Virginia, USA, seismic zone: evidence for possible climatic controls. Tectonophysics 186, 193–214.

Erhardt, W., 1931. Der Staufen: Geologische Aufnahme der Berge zwischen Reichenhall und Inzell. Wiss. Veröffentlichungen d. Deutschen u. Österreichischen Alpenvereins, vol. 11, p. 52.

Ferreira, J.M., Oliveira, R.T., Assumpcao, M., Moreira, J.A.M., Pearce, R.G., Takeya, M.K., 1995. Correlation of seismicity and water level in the Acu Reservoir; an example from Northeast Brazil. Bull. Seismol. Soc. Am. 85 (5), 1483–1489.

Fremount, M.-J., Malone, S.D., 1987. High precision relative localization of earthquakes at Mount St. Helens, Washington. J. Geophys. Res. 92 (B10), 10223–10236.

Fuchs, T., Rapp, J., Rudolf, B., 1999. Klimastatusbericht 1999. Deutschen Wetterdienst, Offenbach/Main, Ch. Niederschlagsanalyse zum Pfingsthochwasser 1999 im Einzugsgebiet von Donau und Bodensee, pp. 26–34.

Giessberger, H., 1918. Das Reichenhaller Einsturzbeben vom 19. November 1910. Königl. bayer. Akademie der Wissenschaften, München, Sitzungsberichte, Mathem.-physikal. Klasse, pp. 221–258.

Glaser, S., 2004. Der Hochstaufen 1349. In: Stautz, G. (Ed.), Münchner Höhlengeschichte II. 50 Jahre Verein für Höhlenkunde in München e.V. VHM, München, pp. 291–295.

Hainzl, S., Ogata, Y., 2005. Detecting fluid signals in seismicity data through statistical earthquake modeling. J. Geophys. Res. 110 (B9), B05S07, doi:10.1029/2004JB003247.

Harris, R.A., 1998. Introduction to special section: stress triggers, stress shadows, and implications for seismic hazard. J. Geophys. Res. 103 (12), 24347–24358.

Henrich, R., Zankl, H., 1981. Die Geologie des Hochstaufenmassivs in den Nördlichen Kalkalpen. Verh. Geol. Bundesanst. (Wien) 2, 31–57.

Hill, P., 1977. A model for earthquake swarms. J. Geophys. Res. 82, 1347–1352.

Howells, L., 1974. The time for a significant change of pore pressure. Eng. Geol. 8, 135–138.

Hubbert, M., Rubey, W., 1959. Role of fluid pressure in mechanics of overthrust faulting: I. Mechanics of fluid-filled porous solids and its application to overthrust faulting. Geol. Soc. Amer. Bull. 70 (2), 115–166.

King, G.C.P., Stein, R.S., Lin, J., 1994. Static stress changes and the triggering of earthquakes. Bull. Seismol. Soc. Am. 84, 935–953.

Kissling, E., Ellsworth, W., Eberhart-Phillips, D., Kradolfer, U., 1994. Initial reference models in local earthquake tomography. J. Geophys. Res. 99 (B10), 19635–19646.

Kodaira, S., Idaka, T., Kato, A., Park, J., Iwasak, T., Kaneda, Y., 2004. High pore fluid pressure may cause silent slip in the Nankai Trough. Science 304, 1295–1298.

Kümpel, H.-J., 1991. Poroelasticity: parameters reviewed. Geophys. J. Int. 105, 783–799.

Lee, M., Wolf, L.W., 1998. Analysis of fluid pressure propagation in heterogeneous rocks: implications for hydrologically-induced earthquakes. Geophys. Res. Lett. 25 (13), 2329–2332.

Lee, W.H.K., Lahr, J.C., 1975. Hypo71 (revised): a computer program for determining hypocenter, magnitude, and first motion of local earthquakes. Open-file report, vol. 75–311, p. 114.

Manga, M., Brodsky, E.E., Boone, M., 2003. Response of streamflow to multiple earthquakes. Geophys. Res. Lett. 30, 1214, doi:10.1029/2002GL016618.

Miller, S.A., Collettini, C., Chiaraluce, L., Cocco, M., Barchi, M., Kaus, B.J.P., 2004. Aftershocks driven by a high-pressure CO_2 source at depth. Nature 427, 724–727.

Mogi, K., 1963. Some discussions on aftershocks, foreshocks and earthquake swarms — the fracture of a semi infinite body caused

by inner stress origin and its relation to the earthquake phenomena. Bull. Earthq. Res. Inst. Univ. Tokyo 41, 615–658.
Muco, B., 1995. The seasonality of Albanian earthquakes and cross-correlation with rainfall. Phys. Earth Planet. Inter. 88, 285–291.
Muco, B., 1999. Statistical investigation on possible seasonality of seismic activity and rainfall-induced earthquakes in Balkan area. Phys. Earth Planet. Inter. 114, 119–127.
Munich Re Group, 2003. topics: Annual review: Natural catastrophes 2002. Vol. 10th year. Münchener Rückversicherungsgesellschaft, Munich, Germany, Ch. The summer floods in Europe —A millennium flood?, pp. 17–25.
Neuzil, C., 2003. Hydromechanical coupling in geologic processes. Hydrogeol. J. 11, 41–83.
Nöthen, M., 1981. Untersuchung der lokalen seismischen Aktivität im Raum Bad Reichenhall. Diploma thesis, University of Munich.
Nur, A., Booker, J., 1972. Aftershocks caused by pore fluid flow? Science 175, 885–887.
Parotidis, M., Rothert, E., Shapiro, S.A., 2003. Pore-pressure diffusion: a possible triggering mechanism for the earthquake swarm 2000 in Vogtland/NW-Bohemia, Central Europe. Geophys. Res. Lett. 30 (20), 2075, doi:10.1029/2003GL018110.
Parotidis, M., Shapiro, S.A., Rothert, E., 2005. Evidence for triggering of the Vogtland swarms 2000 by pore pressure diffusion. J. Geophys. Res. 110 (B9), 2075, doi:10.1029/2004JB003267.
Poupinet, G., Ellsworth, W., Frechet, J., 1984. Monitoring velocity variations in the crust using earthquake doublets: an application to the Calaveras Fault, California. J. Geophys. Res. 89 (B7), 5719–5731.
Prejean, S.G., Hill, P.D., Brodsky, E.E., Hough, S.E., Johnston, M.J.S., Malone, S.D., Oppenheimer, D.H., Pitt, A.M., Richards-Dinger, K. D., 2004. Remotely triggered seismicity on the United States west coast following the Mw 7.9 Denali Fault earthquake. Bull. Seismol. Soc. Am. 94 (6B), 348–359.
Rietbrock, A., Scherbaum, F., 1998. The GIANT analysis system (Graphical Interactive Aftershock Network Toolbox). Seismol. Res. Lett. 69, 40–45.
Roeloffs, E.A., 1988. Fault stability changes induced beneath a reservoir with cyclic variations in water level. J. Geophys. Res. 93 (12), 2107–2124.
Roeloffs, E.A., Sneed, M., Galloway, D.L., Sorey, M.L., Farrar, C.D., Howle, J.F., Hughes, J., 2003. Water-level changes induced by local and distant earthquakes at Long Valley caldera, California. J. Volcanol. Geotherm. Res. 127, 269–303.
Roth, P., Pavoni, N., Deichmann, N., 1992. Seismotectonic of the eastern Swiss Alps and evidence for precipitation-induced variations of seismic activity. Tectonophysics 207, 183–197.
Rothert, E., Shapiro, S.A., 2003. Microseismic monitoring of borehole fluid injections: data modeling and inversion for hydraulic properties of rocks. Geophysics 68 (2), 685–689.
Saar, M.O., Manga, M., 2003. Seismicity induces by seasonal groundwater recharge at Mt. Hood, Oregon. Earth Planet. Sci. Lett. 214, 605–618.
Schmedes, E., 1979. Die seismische Aktivität im Raum Bad Reichenhall. Geol. Jahrb. C22, 91–102.
Scholz, C.H., 1994. The Mechanics of Earthquakes and Faulting. Cambridge University Press.
Schwarzmann, A., 1996. Untersuchungen der seismischen Aktivität im Raum Bad Reichenhall. Diploma Thesis, University of Munich.
Segall, P., 1985. Stress and subsidence resulting from subsurface fluid withdrawal in the epicentral region of the 1983 Coalinga earthquake. J. Geophys. Res. 90 (9), 6801–6816.
Shapiro, S.A., Huenges, E., Borm, G., 1997. Estimating the crust permeability from fluid-injection-induced seismic emission at the KTB site. Geophys. J. Int. 131, F15–F18.
Shapiro, S.A., Patzig, R., Rothert, E., 2003. Triggering of seismicity by pore pressure perturbations: permeability-related signatures of the phenomenon. Pure Appl. Geophys. 160, 1051–1066.
Sleep, N., Blanpied, M.L., 1992. Creep, compaction and the weak rheology of major faults. Nature 359, 687–692.
Sykes, L., 1970. Earthquake swarms and sea-floor spreading. J. Geophys. Res. 75, 6598–6611.
Talwani, P., 2000. Seismogenic properties of the crust inferred from recent studies of reservoir-induced seismicity — application to Koyna. Curr. Sci. India 79 (9), 1327–1333.
Terzaghi, K., 1923. Die Berechnung der Durchlässigkeitziffer des Tones aus dem Verlauf der hydrodymanischen Spannungserscheinungen. Akademie d. Wissenschaften Wien, Sitzungsberichte, Mathem.-naturwiss. Klasse, Part IIa, vol. 132 (3/4), pp. 125–138.
Tollmann, A., 1976. Der Bau der Nördlichen Kalkalpen. Orogene Stellung und regionale Tektonik, vol. 3. Deuticke, Wien.
Ventura, G., Vilardo, G., 1999. Seismic-based estimate of hydraulic parameters at Vesuvius volcano. Geophys. Res. Lett. 26, 887–890.
Wang, H.F., 2000. Theory of linear poroelasticity with applications to geomechanics and hydrogeology. Princeton University Press.
Weede, M., 2002. Die Geologie des Hochstaufen unter besonderer Berücksichtigung der Massenbewegungen. Diploma Thesis, Technical University of Munich.
Will, M., 1975. Refraktions-Seismik im Nordteil der Ostalpen zwischen Salzach und Inn, 1970–1974; Messungen und deren Interpretation. PhD thesis, LMU Munich.
Wolf, L., Rowe, C., Horner, R., 1997. Periodic seismicity near Mt. Ogden on the Alaska–British Columbia border: a case for hydrologically triggered earthquakes? Bull. Seismol. Soc. Am. 87 (6), 1473–1483.
Yamashita, T., 1999. Pore creation due to fault slip in a fluid-permeated fault zone and its effects on seismicity: generation mechanism of earthquake swarms. Pure Appl. Geophys. 155, 625–647.
Zankl, H., Schell, O., 1979. Der geologische Bau des Talkessels von Bad Reichenhall (Nördliche Kalkalpen). Geol. Jahrb. 22.
Zhang, H., Thurber, C.H., 2003. Double-difference tomography: method and its application to the Hayward Fault, California. Bull. Seismol. Soc. Am. 93 (5), 1875–1889.